Supplementary Materials

Enhanced CO_2 Photoreduction over Bi_2Te_3/TiO_2 Nanocomposite via a Seebeck Effect

Yiming Lei [1,2], Zewei Jia [1,2], Huilin Hu [1,2], Lequan Liu [1,2], Jinhua Ye [1,2,3] and Defa Wang [1,2,*]

[1] TJU-NIMS International Collaboration Laboratory, Key Laboratory of Advanced Ceramics and Machining Technology (Ministry of Education) and Tianjin Key Laboratory of Composite and Functional Materials, School of Material Science and Engineering, Tianjin University, Tianjin 300072, China
[2] Collaborative Innovation Centre of Chemical Science and Engineering (Tianjin), Tianjin 300072, China
[3] International Center for Materials Nanoarchitectonics (WPI-MANA), National Institute for Materials Science (NIMS), 1-1 Namiki, Tsukuba 305-0044, Japan
* Correspondence: defawang@tju.edu.cn; Tel.: +86-22-27405065

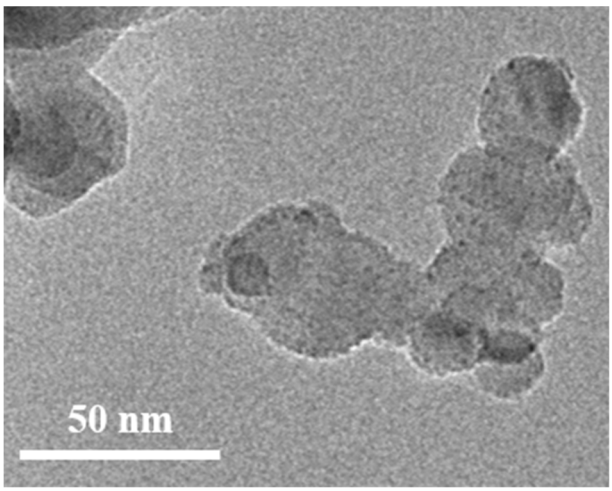

Figure S1. TEM image of pBT(2)/P25.

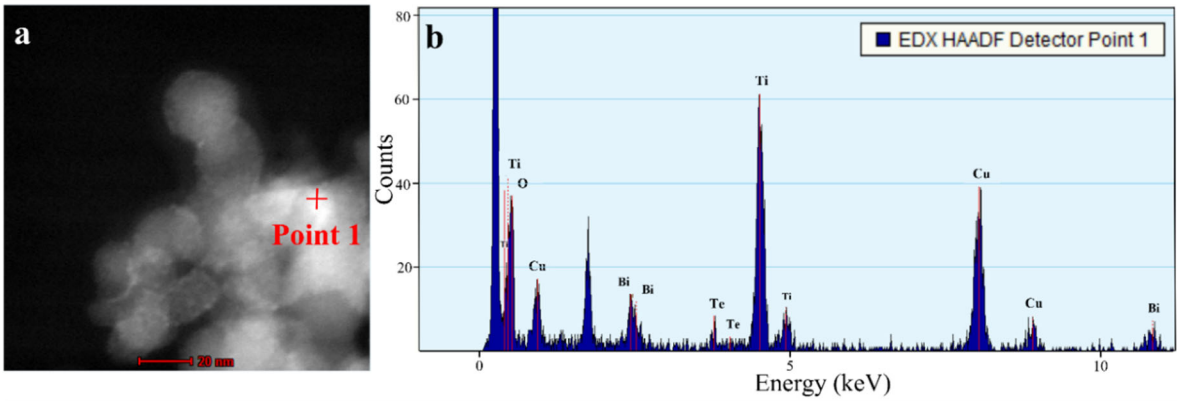

Figure S2. (**a**) High-angle annular dark-field (HAADF) TEM image, and (**b**) EDS analysis of pBT(2)/P25.

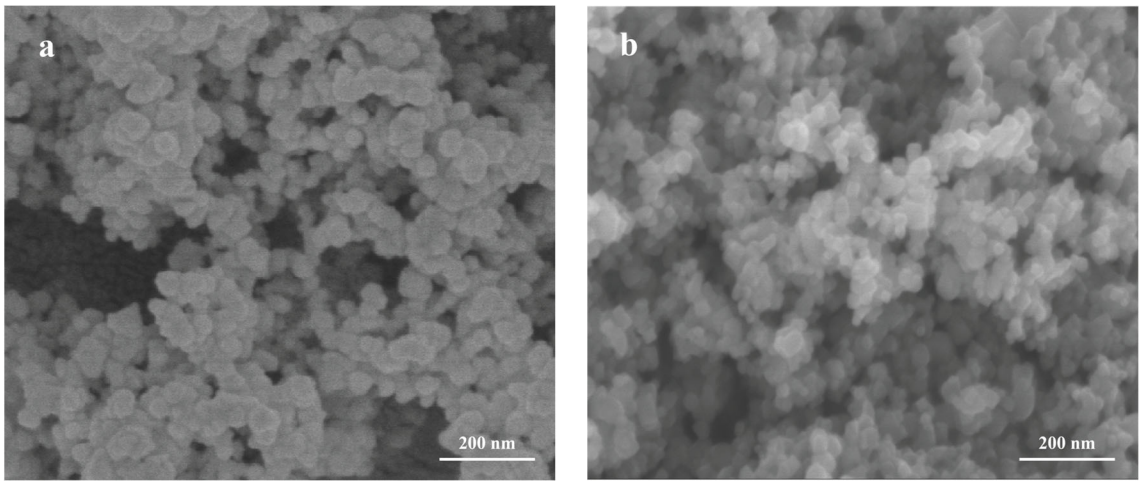

Figure S3. SEM images of (**a**) P25 and (**b**) pBT(2)/P25

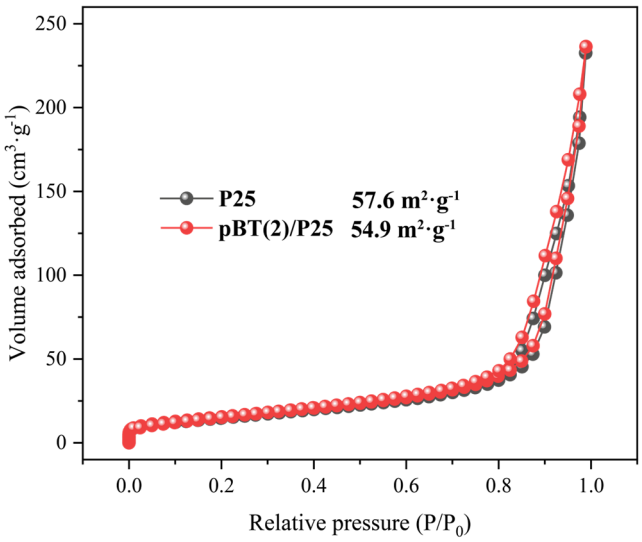

Figure S4. N_2 sorption isotherms of P25 and pBT(2)/P25.

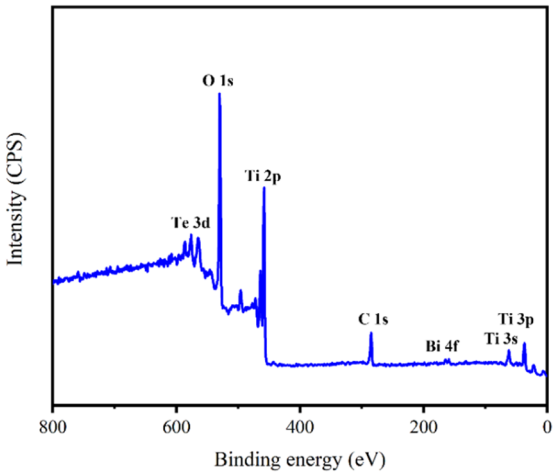

Figure S5. XPS survey spectra of pBT(2)/P25.

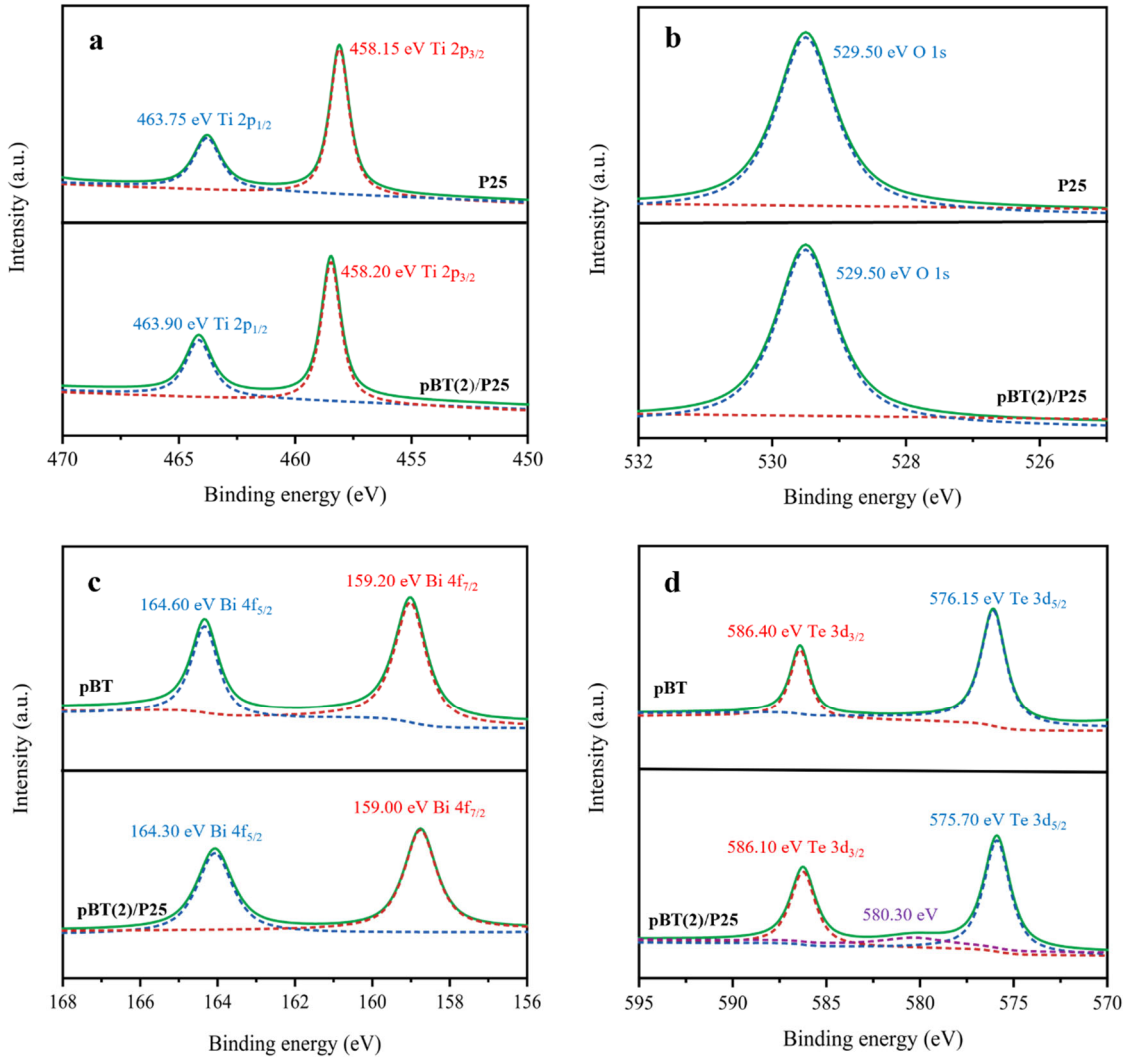

Figure S6. High-resolution XPS spectra of (**a**) Ti 2p, (**b**) O 1s in pure P25 and pBT(2)/P25; (c) Bi 4f, and (**d**) Te 3d in pure pBT and pBT(2)/P25.

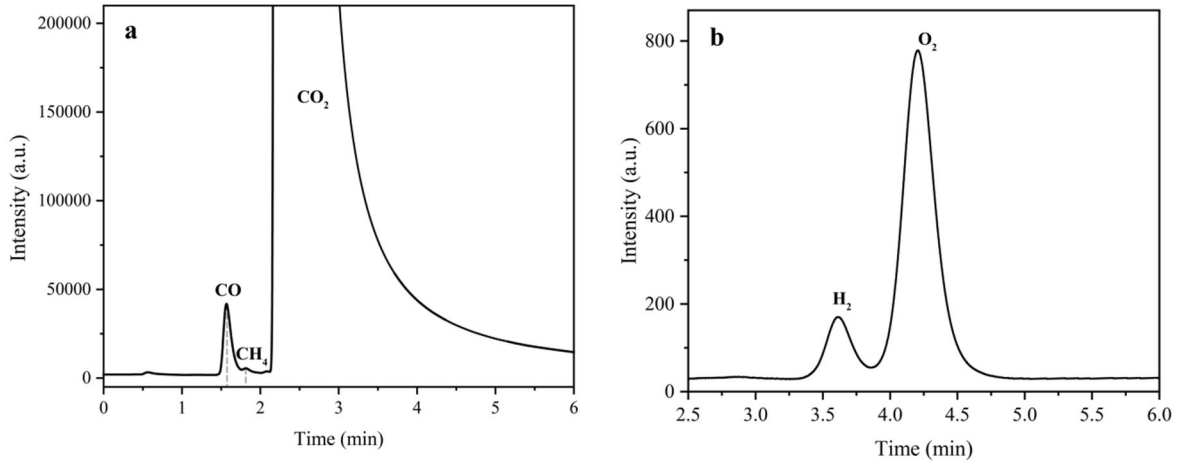

Figure S7. The typical GC spectra showing (**a**) the main product CO and a trace amount of CH_4 (note 1); (**b**) H_2 and O_2 in CO_2 photoreduction over pBT(2)/P25 (note 2).

Note 1: The gaseous sample (0.5 mL) was taken from the reaction vessel and analyzed on a gas chromatograph (GC-2014, Shimadzu, Japan) equipped with a flame ionization detector (FID) and methanizer for analysis of CO, CH_4, and CO_2 using N_2 as the carrier gas.

Note 2: The evolved O_2 and H_2 were analyzed using an online gas chromatograph (GC-2014C, Shimadzu, Japan) equipped with a thermal conductivity detector (TCD) using Ar as the carrier gas.

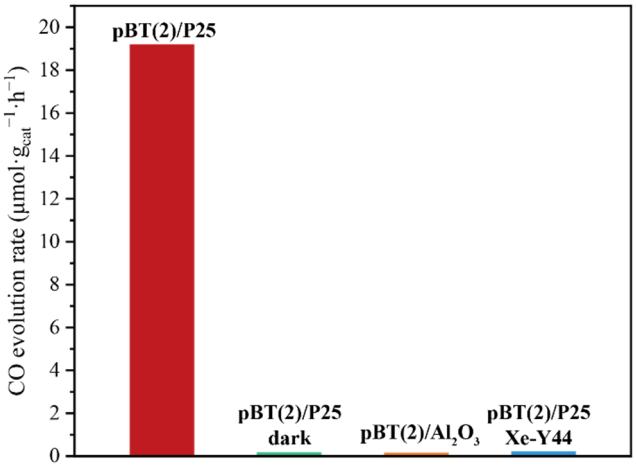

Figure S8. CO evolution rates over pBT(2)/P25 and pBT(2)/Al_2O_3.

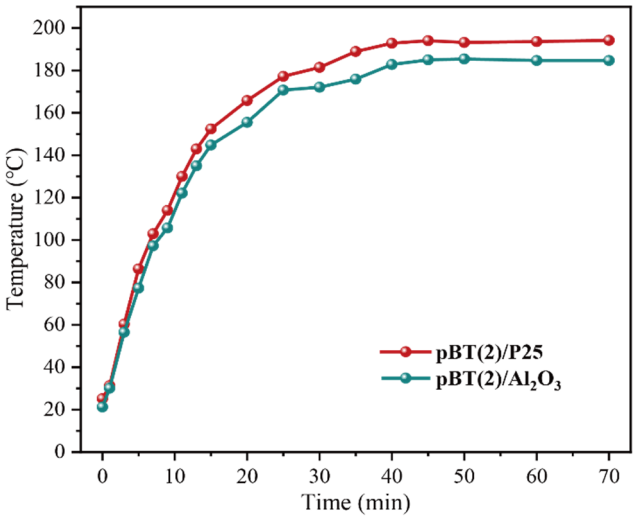

Figure S9. In-situ monitoring of the photothermal temperatures over pBT(2)/P25 and pBT(2)/Al_2O_3 under a 300 W full-arc Xe lamp irradiation.

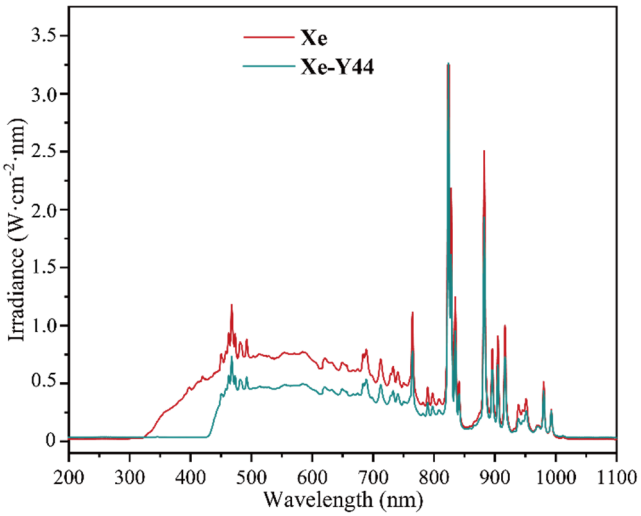

Figure S10. Light spectra of the full-arc Xe lamp and Xe lamp with a Y44 cutoff optical filter.

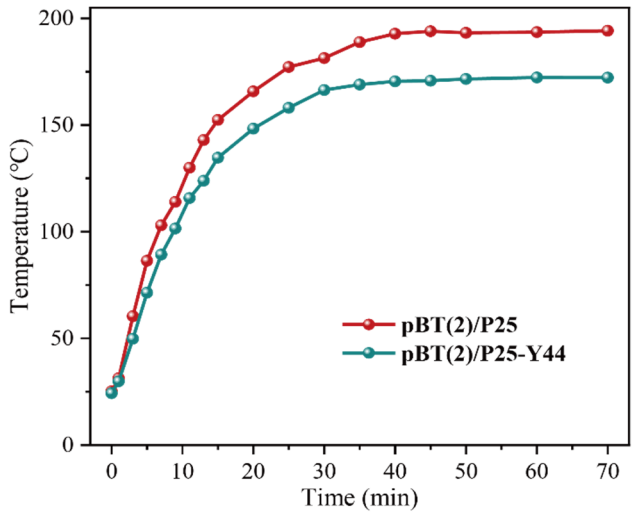

Figure S11. In-situ monitoring of the photothermal temperatures over pBT(2)/P25 under a 300 W full arc Xe lamp irradiation with and without a Y44 cutoff optical filter.

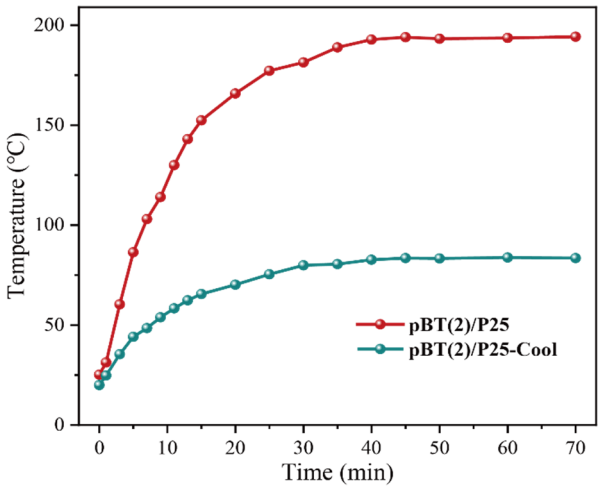

Figure S12. In-situ monitoring of the photothermal temperatures over pBT(2)/P25 under photothermal and cooling conditions. Photothermal condition: the reaction cell was irradiated by 300 W full-arc Xe lamp. Cooling condition: the reaction cell was placed in a basin containing cold water under Xe lamp irradiation.

Table S1. Temperatures over P25 and pBT(x)/P25 after CO_2 photoreduction under photothermal and cooling conditions.

	Photothermal condition (°C)	Cooling condition (°C)
P25	129	74
pBT(1)/P25	161	79
pBT(2)/P25	191	84
pBT(3)/P25	223	86
pBT(4)/P25	255	89

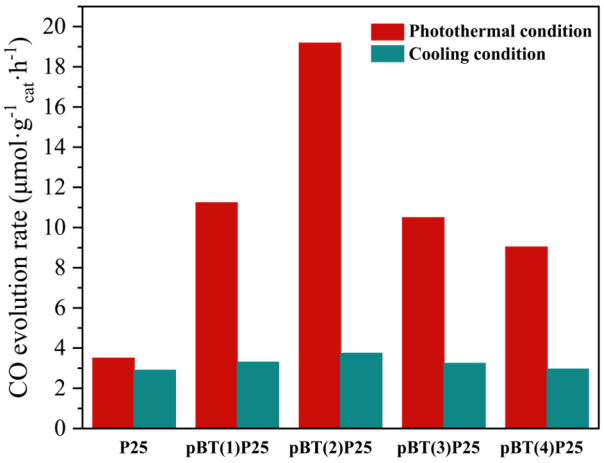

Figure S13. CO evolution rates over P25 and pBT(x)/P25 under photothermal and cooling conditions.

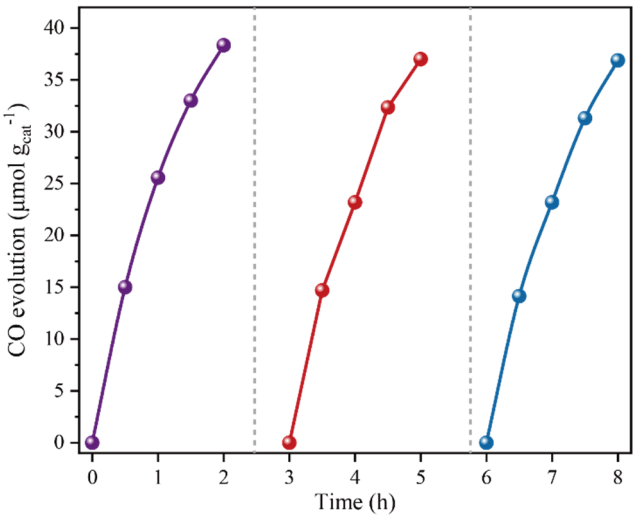

Figure S14. Three cycles of CO_2 photoreduction over pBT(2)/P25.

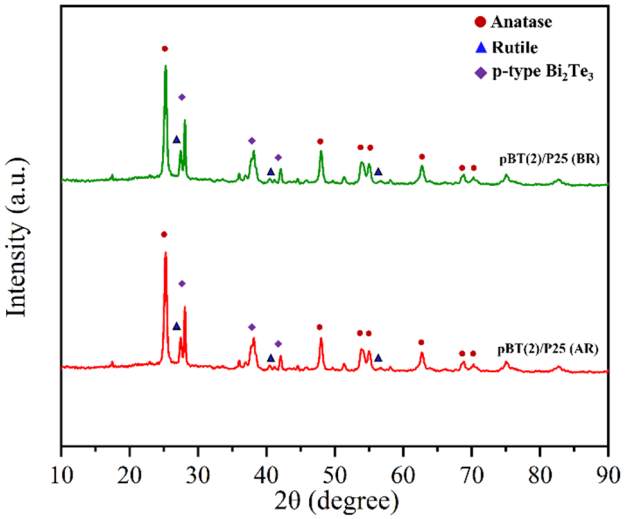

Figure S15. XRD patterns of pBT(2)/P25 before reaction (BR) and after reaction (AR).

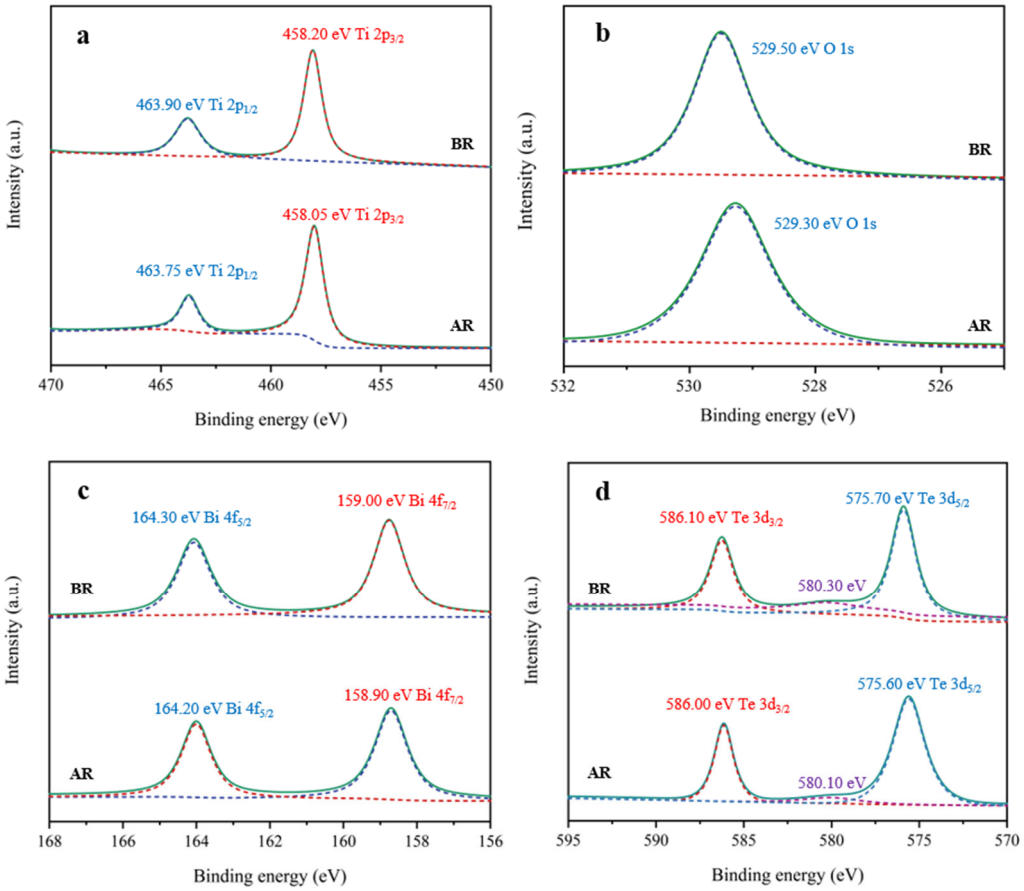

Figure S16. High-resolution XPS spectra of (**a**) Ti 2p, (**b**) O 1s, (**c**) Bi 4f, and (**d**) Te 3d in pBT(2)/P25 before and after reaction cycles (denoted as BR and AR).

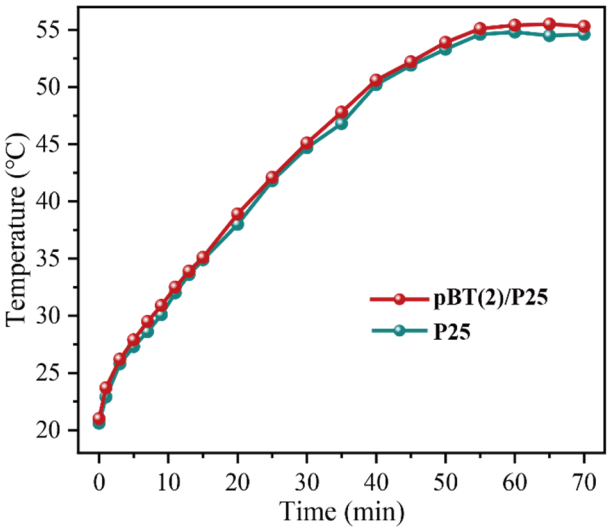

Figure S17. In-situ monitoring of the surface temperatures of P25 and pBT(2)/P25 photoanodes immersed in K_2SO_4 electrolyte during PEC measurement under a 300 W full-arc Xe lamp irradiation.

Table S2. Surface temperatures of P25 and pBT(x)/P25 photoanodes in K_2SO_4 electrolyte

	CO_2 reduction (°C)	PEC measurments (°C)
P25	129	54
pBT(1)/P25	161	54
pBT(2)/P25	191	55
pBT(3)/P25	223	55
pBT(4)/P25	255	55

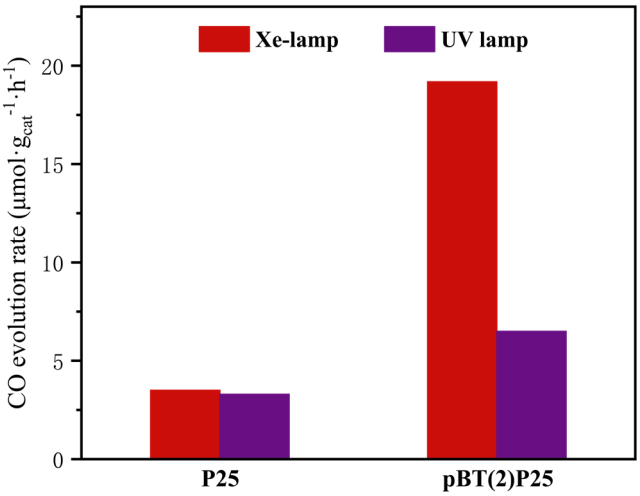

Figure S18. CO evolution rates over P25 and pBT(x)/P25 under Xe lamp and UV lamp irradiation.

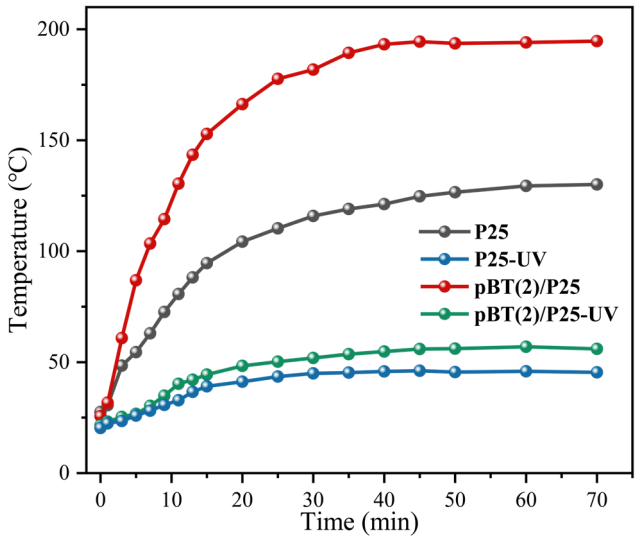

Figure S19. In-situ monitoring of the photothermal temperatures over P25 and pBT(2)/P25 under Xe lamp and UV lamp (denoted as P25-UV and pBT(2)/P25-UV) irradiation.

Table S3 Comparison of CO_2 photoreduction performance over various TiO_2-based photocatalysts

Photocatalyst	Reaction condtion	Light source	CO_2 reduction product evolution rate	Reference
pBT/P25	50 mg catalysts, 3 ml H_2O, and CO_2	300 W Xe-lamp	CO: 19.2 $\mu mol \cdot g_{cat}^{-1} \cdot h^{-1}$ CH_4: 0.4 $\mu mol \cdot g_{cat}^{-1} \cdot h^{-1}$	This work
W-doped TiO_2	50 mg catalysts, 2 ml H_2O, and CO_2	150 W UV-lamp	CO: 0.056 $\mu mol \cdot g_{cat}^{-1} \cdot h^{-1}$	*Nanoscale* **2020**, *12*, 17245-17252.
Ag/TiO_2	50 mg catalysts, 40 ml H_2O, and CO_2	300 W Xe-lamp	CO: 0.575 $\mu mol \cdot g_{cat}^{-1} \cdot h^{-1}$	*Chem. Eng. J.* **2021**, *410*, 128397.
Ag/TiO_2−Zeolite TS-1	7 mg catalysts, 1 ml H_2O, and CO_2	300 W Xe-lamp	CO: 8.1 $\mu mol \cdot g_{cat}^{-1} \cdot h^{-1}$ CH_4: 1.7 $\mu mol \cdot g_{cat}^{-1} \cdot h^{-1}$	*J Hazard. Mater.* **2021**, *403*, 124019
F-TiO_{2-x}	50 mg catalysts, 1 ml H_2O, and CO_2	300 W Xe-lamp, AM 1.5 optical filter	CO: 6.5 $\mu mol \cdot g_{cat}^{-1} \cdot h^{-1}$ CH_4: 4.3 $\mu mol \cdot g_{cat}^{-1} \cdot h^{-1}$	*Nano Letters* **2018**, *18*, 3384-3390.
Mo/TiO_2	100 mg catalysts, 20 μl H_2O, and 20 ml CO_2	300 W Xe-lamp	CO: 0.3 $\mu mol \cdot g_{cat}^{-1} \cdot h^{-1}$ CH_4: 0.2 $\mu mol \cdot g_{cat}^{-1} \cdot h^{-1}$	*J. CO_2 Util.* **2020**, *38*, 1-9.
Au/TiO_2/$BiVO_4$	200 mg catalysts, 10 ml H_2O, and CO_2	300 W Xe-lamp	CO: 2.5 $\mu mol \cdot g_{cat}^{-1} \cdot h^{-1}$ CH_4: 7.5 $\mu mol \cdot g_{cat}^{-1} \cdot h^{-1}$	*J. Mater. Chem. A* **2018**, *6*, 11838-11845.
TiO_2/$CsPbBr_3$	10 mg catalysts, 30 mL acetonitrile+100 μL H_2O, and CO_2	300 W Xe-lamp	CO: 4.0 $\mu mol \cdot g_{cat}^{-1} \cdot h^{-1}$	*Nat. Commun.* **2020**, *11*, 4613.
TiO_2/C_3N_4/Ti_3C_2	30 mg catalysts, 0.84 mg $NaHCO_3$, 0.3 mL 2 mol L^{-1} H_2SO_4, and CO_2	350 W Xe-lamp	CO: 4.4 $\mu mol \cdot g_{cat}^{-1} \cdot h^{-1}$ CH_4: 1.2 $\mu mol \cdot g_{cat}^{-1} \cdot h^{-1}$	*Appl. Catal. B* **2020**, *272*, 119006.

References

1. Li, Y.; Walsh, A. G.; Li, D.; Do, D.; Ma, H.; Wang, C.; Zhang, P.; Zhang, X. W-Doped TiO_2 for photothermocatalytic CO_2 reduction. *Nanoscale* **2020**, *12*, 17245-17252.
2. Li, G.; Sun, Y.; Zhang, Q.; Gao, Z.; Sun, W.; Zhou, X. Ag quantum dots modified hierarchically porous and defective TiO_2 nanoparticles for improved photocatalytic CO_2 reduction. *Chem. Eng. J.* **2021**, *410*, 128397.
3. Sun, Y.; Li, G.; Gong, Y.; Sun, Z.; Yao, H.; Zhou, X. Ag and TiO_2 nanoparticles co-modified defective zeolite TS-1 for improved photocatalytic CO_2 reduction. *J Hazard. Mater.* **2021**, *403*, 124019.
4. Xing, M.; Zhou, Y.; Dong, C.; Cai, L.; Zeng, L.; Shen, B.; Pan, L.; Dong, C.; Chai, Y.; Zhang, J.; Yin, Y. Modulation of the reduction potential of TiO_{2-x} by fluorination for efficient and selective CH_4 generation from CO_2 photoreduction. *Nano Letters* **2018**, *18*, 3384-3390.
5. Feng, S.; Zhao, J.; Bai, Y.; Liang, X.; Wang, T.; Wang, C. Facile synthesis of Mo-doped TiO_2 for selective photocatalytic CO_2 reduction to methane: promoted H_2O dissociation by Mo doping. *J. CO_2 Util.* **2020**, *38*, 1-9.
6. Bian, J.; Qu, Y.; Zhang, X.; Sun, N.; Tang, D.; Jing, L. Dimension-matched plasmonic $Au/TiO_2/BiVO_4$ nanocomposites as efficient wide-visible-light photocatalysts to convert CO_2 and mechanistic insights. *J. Mater. Chem. A* **2018**, *6*, 11838-11845.
7. Xu, F.; Meng, K.; Cheng, B.; Wang, S.; Xu, J.; Yu, J. Unique S-scheme heterojunctions in self-assembled $TiO_2/CsPbBr_3$ hybrids for CO_2 photoreduction. *Nat. Commun.* **2020**, *11*, 4613.
8. He, F.; Zhu, B.; Cheng, B.; Yu, J.; Ho, W.; Macyk, W. 2D/2D/0D $TiO_2/C_3N_4/Ti_3C_2$ MXene composite S-scheme photocatalyst with enhanced CO_2 reduction activity. *Appl. Catal. B* **2020**, *272*, 119006.